

Cluster properties of heavy nuclei predicted with the Barcelona-Catania-Paris-Madrid energy density functional

Samuel A. Giuliani^{1,2*} and Luis M. Robledo^{1,3*}

^{1*}Departamento de Física Teórica and CIAFF, Universidad Autónoma de Madrid, c. Francisco Tomás y Valiente 7, Cantoblanco, 28049, Madrid, Spain.

²Department of Physics, Faculty of Engineering and Physical Sciences, University of Surrey, Guildford, GU2 7XH, United Kingdom.

³Center for Computational Simulation, Universidad Politécnica de Madrid, Campus Montegancedo, Boadilla del Monte, 28660, Madrid, Spain.

*Corresponding author(s). E-mail(s): samuel.giuliani@uam.es; luis.robledo@uam.es;

Abstract

We study the cluster emission properties of ^{224}Ra and ^{238}Pu employing the Barcelona-Catania-Paris-Madrid (BCPM) energy density functional (EDF). Starting from two-dimensional potential energy surfaces, coexisting fission paths are identified. A fission valley located at large octupole deformations, corresponding to a highly-asymmetric mass distribution, is found in both nuclei. As the corresponding fragments are dominated by the presence of ^{208}Pb , we can relate this fission path to the emergence of cluster emission. Using the octupole moment as collective degree of freedom, we compute the cluster decay half-lives and study the impact of collective inertias, pairing strength and collective zero-point energy. The agreement with experimental data resembles the results obtained for spontaneous fission half-lives, indicating the capability of BCPM to consistently describe a large variety of fission phenomena, including cluster emission.

Keywords: Cluster decay, BCPM, spontaneous fission, half-lives, ^{224}Ra , ^{238}Pu .

1 Introduction

The phenomenon of cluster decay, or cluster radioactivity, consists in the spontaneous emission of fragments with an intermediate mass between fission and α decay. Originally postulated by Sandulescu *et al.* in 1980 [1] and experimentally observed by Rose and Jones four years later [2], this decay is driven by the emission of one fragment in the neighborhoods of the doubly magic nucleus ^{208}Pb . From a theoretical point of view, cluster radioactivity can be described as a

highly-asymmetric fission mode, where the fragments emerge as the consequence of the quantum mechanical tunneling through the potential barrier of the compound nucleus. Given the extreme mass asymmetries characterizing this decay, the odd-parity octupole moment can be used as driving coordinate. Therefore, cluster emission studies explore octupole deformation not only in the traditional ground state regime, but also in the extreme elongations required for the formation of a well defined neck that defines scission point and fragment emission properties. Due to this, cluster decay has been the subject of several

experimental measurements [3–10] and microscopic studies based on effective nucleon-nucleon interactions [11–15], with a renewed interest in the latest years arising from its predicted presence in the super-heavy landscape [16–18].

The Barcelona Catania Paris Madrid (BCPM) [19] functional was originally developed to describe with good accuracy binding energies and radii of finite nuclei. Large scale mean-field Hartree-Fock-Bogoliubov (HFB) calculations revealed that deformation properties of the functional are at the level of other interactions such as Gogny D1S or DIM. This property opens up the door to the use of BCPM in fission studies, and more specifically to describe spontaneous fission lifetimes [20–22]. One of the most useful features of BCPM is its relatively low computational cost, specially when compared with finite range interactions like Gogny. This feature makes possible large-scale fission calculations like the ones required in stellar nucleosynthesis studies, including fission recycling of super-heavy neutron rich nuclei [23].

Given the success of BCPM in traditional fission studies, it seems pertinent to explore the ability of the functional to describe very asymmetric fission modes like the one taking place in cluster emission in actinides. This decay provides an optimal case study for assessing the capability of microscopic models to properly reproduce shell structure properties of parent and daughters nuclei at large deformations, as well as the collective inertias required in the calculation of cluster decay half-lives. In this work, we present the results obtained for two different nuclei: ^{224}Ra and ^{238}Pu . The former is one of the first cluster emitters detected in laboratory [4], and represents a canonical standard for studies concerning cluster emission. The latter is a well known case of cluster emission observed in the transactinide region [6], and allows the exploration of cluster phenomena in heavier systems. In this work, the cluster path is identified by computing the evolution of the energy as a function of quadrupole and octupole deformation. Cluster emission lifetimes are thus obtained using the octupole moment as collective degree of freedom. Despite the sensitivity of the lifetimes with respect to the different quantities entering the collective action integral, a good agreement with experimental data is found.

The paper is structured as follows. In Section 2, the theoretical framework employed in the calculation of the cluster decay half-lives is outlined. In Section 3, fission pathways and cluster decay half-lives predicted by BCPM are discussed. Conclusions are summarized in Section 4, together with an outlook on future work.

2 Methods

The self-consistent description of highly asymmetric fission is based on the HFB method with constraining operators [24, 25]. In the HFB method, the many-body wavefunction $|\Psi\rangle$ is defined as the vacuum to all the annihilation quasiparticle operators β_μ . Nuclear states are thus obtained by minimizing the Routhian with constraints on the neutron N and proton Z particle number, and the mass multipole moments $Q_{\mu\nu}$

$$\hat{H}' = \hat{H} - \sum_{\tau=N,Z} \lambda_\tau \hat{N}_\tau - \sum_{\mu=1,2,3} \lambda_\mu \hat{Q}_{\mu 0}, \quad (1)$$

being \hat{H} the HFB Hamiltonian. The independent λ_i quantities are determined by the condition that the gradient of the Routhian has to be orthogonal to the gradient of the constraints. In this work, we impose constraints on the axially symmetric quadrupole (Q_{20}), and octupole (Q_{30}) moments, defined as

$$\hat{Q}_{20} = \hat{z}^2 - \frac{1}{2}(\hat{x}^2 + \hat{y}^2); \quad (2a)$$

$$\hat{Q}_{30} = \hat{z}^3 - \frac{3}{2}(\hat{x}^2 + \hat{y}^2)\hat{z}. \quad (2b)$$

Higher multiplicities are self-consistently adjusted in order to minimize the total energy, e.g. the hexadecapole (Q_{40}) moment related to the development of a fission neck:

$$\hat{Q}_{40} = \hat{z}^4 - 3(\hat{x}^2 + \hat{y}^2)\hat{z}^2 + \frac{3}{8}(\hat{x}^2 + \hat{y}^2)^2. \quad (3)$$

The dipole moment Q_{10} is set to zero to avoid spuriousness associated with the centre-of-mass motion.

The HFB equations are solved using the HFBaxial computer code, which employs an approximate second-order gradient method to

determine the amplitudes of the Bogoliubov transformation to quasiparticles [26]. The quasiparticle operators are expanded in a large deformed axially-symmetric harmonic oscillator (HO) basis, containing states with J_z up to 35/2 and 26 quanta along the z -direction. The HO quantum numbers are restricted by the condition $n_z/q + 2n_\perp + |m| \leq N_0$, with $N_0 = 17$ and $q = 1.5$. This configuration is well suited for describing elongated shapes along the z direction, as those routinely found in fission. The two oscillator lengths characterising the HO bases are chosen as to minimize the energy for each constrained configuration considered.

One of the goals of the present paper is to evaluate the half-lives of spontaneous cluster emission, which can be obtained by means of the Wenzel-Kramers-Brillouin (WKB) method:

$$t_{1/2}(s) = 2.86 \times 10^{-21} [1 + \exp(2S)], \quad (4)$$

being S the collective action computed along the fission path $L(Q_{30})$ [27]

$$S = \frac{1}{\hbar} \int_a^b dQ_{30} \sqrt{2\mathcal{M}(Q_{30})(\mathcal{V}(Q_{30}) - E_0)}. \quad (5)$$

In this work, collective inertias $\mathcal{M}(Q_{30})$ are computed using the perturbative cranking approximation within the adiabatic time-dependent HFB (ATDHFB) [28] and the Gaussian Overlap Approximation to the Generator Coordinate Method (GOA-GCM) [29] formalisms:

$$\mathcal{M}_{\text{ATDHFB}}(Q_{30}) = \hbar^2 \frac{M_{-3}(Q_{30})}{2M_{-1}^2(Q_{30})}; \quad (6a)$$

$$\mathcal{M}_{\text{GOA-GCM}}(Q_{30}) = \hbar^2 \frac{(M_{-2}(Q_{30}))^2}{2M_{-1}^3(Q_{30})}, \quad (6b)$$

being M_{-n} the energy-weighted moments obtained from the one-quasiparticle energies E_μ and the two-quasiparticle zero-hole component of the octupole operator $(Q_{30}^{20})_{\mu\nu}$ (see Appendix E in Ref. [29]):

$$M_{-n}(Q_{30}) = \sum_{\mu\nu} \frac{|(Q_{30}^{20})_{\mu\nu}|^2}{(E_\mu - E_\nu)^n}. \quad (7)$$

The effective potential $\mathcal{V}(Q_{30})$ is obtained by subtracting the rotational and zero-point energy

corrections from the HFB energy

$$\mathcal{V}(Q_{30}) = E_{\text{HFB}}(Q_{30}) - E_{\text{rot}}(Q_{30}) - E_{\text{zpe}}(Q_{30}). \quad (8)$$

In this expression, E_{rot} represents the energy gained by restoring rotational symmetry, which can be effectively computed employing the recipe from Ref. [30]. E_{zpe} is the energy correction associated to quantum fluctuations in the collective degree of freedom Q_{30} , which is computed consistently with the collective inertia scheme [29, 31]:

$$E_{\text{zpe}}^{\text{ATDHFB}}(Q_{30}) = \frac{G(Q_{30})}{2\mathcal{M}_{\text{ATDHFB}}^{-1}(Q_{30})}; \quad (9a)$$

$$E_{\text{zpe}}^{\text{GOA-GCM}}(Q_{30}) = \frac{G(Q_{30})}{2\mathcal{M}_{\text{GOA-GCM}}^{-1}(Q_{30})}, \quad (9b)$$

being the overlaps

$$G(Q_{30}) = \frac{M_{-2}(Q_{30})}{2M_{-1}^2(Q_{30})}. \quad (10)$$

Finally, the action integral defined in Eq. (5) is computed between the classical turning points a and b determined by the condition $\mathcal{V} = E_0$, where E_0 represents the ground-state value of $\mathcal{V}(Q_{30})$ plus the zero-point energy associated to the quantum motion of the nucleus along the collective degrees of freedom. This quantity is usually treated as a free parameter in order to reproduce spontaneous fission lifetimes. In this work, we will study the impact of E_0 in the predicted $t_{1/2}$ by varying its value between 1.0 and 1.5 MeV.

To compute the effective potential energy $\mathcal{V}(Q_{30})$ and collective inertias $\mathcal{M}(Q_{30})$ entering in Eq. (5), we employ the BCPM EDF. For a comprehensive discussion regarding the details and applications of this interaction, we refer to the recent review from Baldo *et al.* [32]. Here, we just recap the basic ingredients of the functional:

- A bulk or volume term is given by two fifth order polynomials of the proton and neutron densities. One of the polynomial is fitted to reproduce the binding energy per nucleon in symmetric nuclear matter, while the other uses the pure neutron matter equation of state. For intermediate situations, a quadratic term proportional to $\beta = \rho_n - \rho_p$ is used to connect both polynomials.

- A surface term, obtained from the Hartree potential of a finite range Gaussian.
- A spin-orbit potential adopting the same form as the ones of Gogny or Skyrme interactions, with a standard spin-orbit strength adapted to the effective mass of BCPM being equal to the bare mass.
- A Coulomb term, with two contributions, one the traditional Hartree term derived from the Coulomb potential and the other the Slater local approximation to Coulomb exchange.

The kinetic energy is computed using the standard quantum mechanic expression.

3 Results

In order to assess the capability of the BCPM interaction to reproduce the main features of cluster decay in heavy nuclei, we follow the strategy of Ref. [13] and study the properties of two representative nuclei: ^{224}Ra and ^{238}Pu .

3.1 Potential energy surfaces and fission paths

Fig. 1 shows the potential energy surface (PES) as a function of the quadrupole Q_{20} and octupole Q_{30} mass moments predicted by BCPM for ^{224}Ra and ^{238}Pu . This plot, representing the evolution of the HFB energy (including the rotational correction) as a function of elongation and mass asymmetry, allows for the identification of the multiple fission paths coexisting in a particular nucleus. Calculations are performed in a grid with a spacing of 2 b in the Q_{20} direction and $2\text{ b}^{3/2}$ in the Q_{30} direction. The harmonic oscillator lengths have been optimized for each configuration. For a better visualization, the predicted ground-state energy has been subtracted from the PES.

We observe that for both nuclei, BCPM predicts a well deformed ground-state configuration: $Q_{20}^{\text{gs}} = 8\text{ b}$ for ^{224}Ra , and $Q_{20}^{\text{gs}} = 14\text{ b}$ for ^{238}Pu . In the case of ^{224}Ra the ground-state is also predicted to break reflection symmetry as $Q_{30}^{\text{gs}} = 4\text{ b}^{3/2}$. Starting from these ground-state configuration, fission paths can be determined by seeking for the maximal decrease in energy. Hence, we find that BCPM predicts the existence of two distinct fission paths. The first one initially proceeds along configurations with small Q_{30} values.

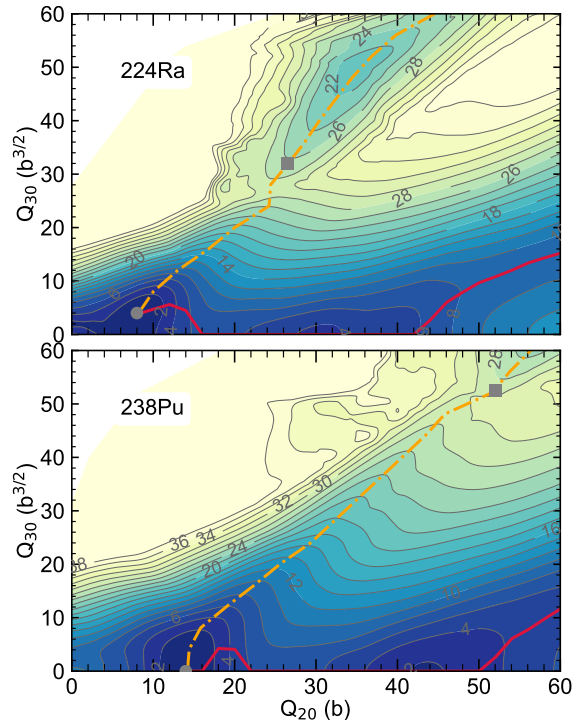


Fig. 1 Evolution of the HFB energy (including rotational correction) in MeV for ^{224}Ra (upper panel) and ^{238}Pu (lower panel), as a function of elongation (Q_{20}) and mass asymmetry (Q_{30}). The ground state configuration of each nucleus is marked with a \bullet symbol. The red solid line represents the traditional elongated fission path. The cluster path is marked with an orange dash-dotted line.

After crossing the fission isomer located at $Q_{20}^{\text{iso}} = 30\text{ b} - 44\text{ b}$, it develops a strong octupole deformation, finally reaching the outer turning point at $(Q_{20}^{\text{out}}, Q_{30}^{\text{out}}) = (136\text{ b}, 40\text{ b}^{3/2})$, and $(Q_{20}^{\text{out}}, Q_{30}^{\text{out}}) = (116\text{ b}, 36\text{ b}^{3/2})$ for ^{224}Ra and ^{238}Pu respectively. This path represents a “traditional” elongated fission mode, where the nucleus splits in two asymmetric fragments, giving raise to the double-humped mass and charge fragment distributions characteristic of several nuclei across the nuclear chart. The blue solid line in Fig. 2 shows the one-dimensional projection of such fission path as a function of the quadrupole moment, together with the evolution of Q_{30} , Q_{40} . Both nuclei show an increase of hexadecapole deformation Q_{40} with increasing Q_{20} , suggesting the development of two fragments connected by a thin fission neck, as typically found in elongated fission modes. The predicted inner barrier height is 6.73 MeV for ^{224}Ra , and 6.79 MeV for ^{238}Pu . We also observe

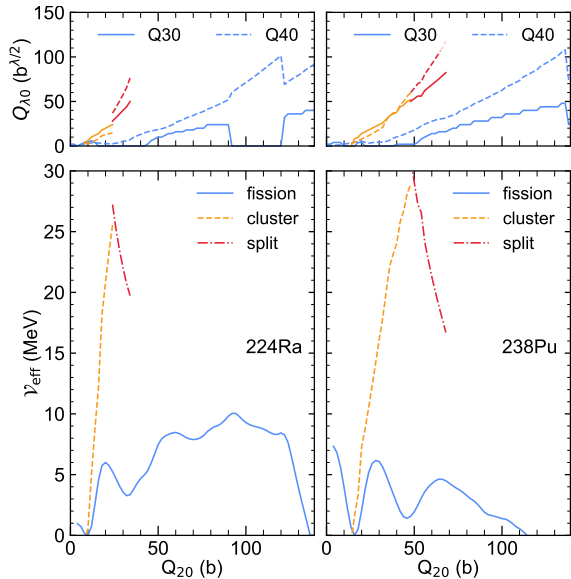


Fig. 2 Fission paths for ^{224}Ra (left panels) and ^{238}Pu (right panels) as a function of elongation. Lower panels: elongated fission path (blue solid lines), cluster path (orange dashed line), and total energy of the emerging cluster fragments (red dash-dotted line), in MeV. Upper panels: evolution of Q_{30} (solid lines) and Q_{40} (dashed lines) mass multipole moments.

that the elongated fission path of ^{224}Ra is particularly wide and has a fission barrier height of 10.76 MeV, indicating that BCPM predicts ^{224}Ra to be stable against fission.

Besides this elongated asymmetric fission path, both PESs in Fig. 1 show the existence of a second fission valley located at very large octupole deformations: $(Q_{20}, Q_{30}) = (34 \text{ b}, 48 \text{ b}^{3/2})$ for ^{224}Ra ; and $(Q_{20}, Q_{30}) = (66 \text{ b}, 76 \text{ b}^{3/2})$ for ^{238}Pu . The octupole moment along the fission path connecting this valley to the ground-state configuration quickly grows with increasing elongation, suggesting the emergence of a highly-asymmetric fission mode. The one dimensional projection of this fission path for both nuclei is plotted in Fig. 2 as a dashed red line. We notice that a saddle point is reached at $Q_{20} = 26 \text{ b}$ for ^{224}Ra , and $Q_{20} = 52$ for ^{238}Pu . At these deformations, the nucleus starts to split into two fragments. For both ^{224}Ra and ^{238}Pu the heavy partner is a spherical nucleus in the vicinity of ^{208}Pb , clearly indicating that the highly-asymmetric fission path found in these nuclei corresponds to a cluster emission. We notice that the energy barrier of cluster decay is above 26 MeV, indicating that the probability of the

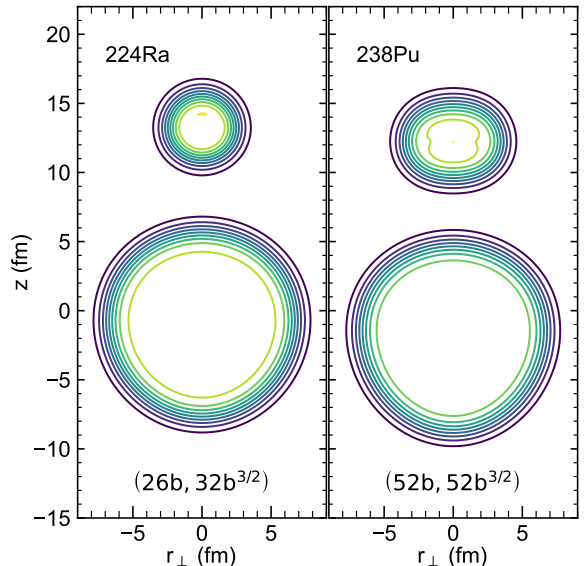


Fig. 3 Spatial mass distribution of ^{224}Ra (left panel) and ^{238}Pu (right panel). The configurations correspond to the \blacksquare symbols plotted in Fig. 1.

nucleus to undergo this decay is much smaller than the one corresponding to the traditional fission decay.

In order to visualize the emerging fragments, Fig. 3 shows the mass distributions of ^{224}Ra and ^{238}Pu at the saddle point of the cluster path. The cluster decay predicted by BCPM for these nuclei are $^{224}\text{Ra} \rightarrow ^{210}\text{Pb} + ^{14}\text{C}$ and $^{238}\text{Pu} \rightarrow ^{208}\text{Pb} + ^{30}\text{Mg}$, in agreement with experimental observations [9]. In both nuclei, fragments' deformation are determined by their ground-state deformation: spherical for ^{14}C , ^{208}Pb and ^{210}Pb , and oblate for ^{30}Mg ($\beta_2 = -0.17$). After overcoming the saddle point of the cluster barrier, i.e., after the splitting of the nucleus into two fragments, the energy of the nucleus starts to decrease with elongation in a parabolic fashion. This is the result of the diminishing Coulomb repulsion between the fragments as they move further apart. The outer turning point of the cluster decay can thus be obtained by following the Coulomb barrier until it falls below the ground-state energy. However, as already discussed by Warda and Robledo [13], we find that this two-fragments configuration quickly saturates the HO basis for large values of the elongation, suggesting that a larger basis should be employed in order to compute the full cluster decay path. Unfortunately, the number of HO shells is limited by numerical accuracy, and cannot be increased

without the emergence of numerical instabilities in the estimation of the matrix elements. This limitation will be addressed in the next section.

3.2 Cluster decay path as a function of Q_{30}

As the cluster path overcomes the energy barrier, it proceeds towards larger deformations by following the bottom of the highly-asymmetric valley described in Sec. 3.1. As shown in Fig. 1, this results in a cluster path placed along a diagonal line in the (Q_{20}, Q_{30}) plane. Hence, a correspondence can be established between increasing elongation and increasing mass asymmetry for these cluster decays. As already proposed in Ref. [13], this proportionality can be exploited in order to parametrize the cluster path as a function of the octupole moment Q_{30} . This change of collective variable is particularly convenient as the PES for a fixed Q_{30} is stiffer than for a fixed Q_{20} , which simplifies the identification of the cluster decay path located at large Q_{30} values.

The one-dimensional cluster path of ^{224}Ra and ^{238}Pu as a function of Q_{30} is plotted in Fig. 4. As in the Q_{20} parametrization of Fig. 2, we notice a fast increase of the energy with increasing Q_{30} . A saddle point is reached at $Q_{30} = 26 \text{ b}^{3/2}$ for ^{224}Ra and $Q_{30} = 52 \text{ b}^{3/2}$ for ^{238}Pu . At these configurations, the nucleus is already split in two fragments, corresponding to the cluster decay described in the previous section. Hence, increasing the octupole moment beyond this point corresponds to a separation of the centre of mass of the fragments, with the consequent diminishment of the total energy due to the decreasing Coulomb repulsion. By approximating the cluster fragments as two homogeneous spheres with charges Z_1 and Z_2 , the Coulomb repulsion energy as a function of the octupole moment can be written as

$$V(Q_{30}) = V_C - Q = e^2 \frac{Z_1 Z_2}{R} - Q, \quad (11)$$

being R the distance between the centers of mass of the fragments, while the decay Q -value can be extracted from the AME2020 database [33]. The relationship between R and the octupole moment can be obtained by approximating the

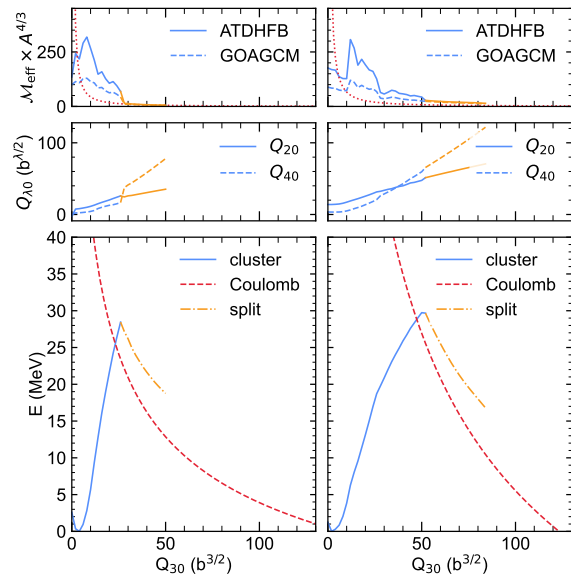


Fig. 4 Fission paths for ^{224}Ra (left panels) and ^{238}Pu (right panels) as a function of mass asymmetry Q_{30} . Lower panels: cluster path (blue solid line), energy of the emerging cluster fragments (orange dash-dotted line), and classical Coulomb repulsion energy (red dashed line), in MeV. Middle panels: evolution of Q_{20} (solid lines) and Q_{40} (dashed lines) mass multipole moments. Upper panels: ATDHFB (6a) (solid lines), GOA-GCM (6b) (dashed lines), and classical Coulomb (14) (dotted line) collective inertias in $\text{MeV}^{-1}\text{b}^{-3}$.

two fragments as spheres with masses A_1 and A_2 :

$$Q_{30} = f_3 R^3, \quad (12)$$

with

$$f_3 = \frac{A_1 A_2}{A} \frac{|A_1 - A_2|}{A}, \quad (13)$$

where A is the mass number of the compound nucleus. The Coulomb repulsion energy from Eq. (11) is plotted in Fig. 4 as a solid red line. At the saddle point, the Coulomb repulsion and the HFB calculations differ by roughly 5 MeV. This discrepancy is slightly larger than the one found in Ref. [13], and can be related to the excitation of the lighter fragment in the presence of the Coulomb field produced and to the shape of the emerging fragments. As a consequence of the saturation of the HO basis discussed in Sec. 3.1, we notice a departure of the HFB calculations from the Coulomb parabola with increasing Q_{30} . As this numerical limitation imposed by the finite size of the basis do not allow a proper calculation of configurations with large values of the octupole

moment, in the next section the cluster decay half-lives will be estimated employing the Coulomb barrier from Eq. (11). For this purpose, one shall rewrite the classical collective inertia for two fragments separated by a distance R in terms of the octupole moment [13]:

$$\mathcal{M}(Q_{30}) = \frac{\mu}{9Q_{30}^{4/3} f_3^{2/3}}, \quad (14)$$

being $\mu = m_n A_1 A_2 / (A_1 + A_2)$ the reduced mass and m_n the nucleon mass. The upper panel of Fig. 4 shows the evolution of the collective inertias from Eqs. (6a), (6b) and (14). The microscopic ATDHFB and GOA-GCM inertias present large fluctuations due to the crossing of single particle levels, which are obviously absent in the classical collective inertias. However, once the parental nucleus splits into two fragments, both microscopic inertias agree to the same asymptotic value.

3.3 Cluster decay half-lives

In order to estimate the spontaneous fission half-lives of cluster decay, we employ the formalism described in Sec. 2. The fission path $L(Q_{30})$ employed in the estimation action integral is obtained by splicing the cluster path (parametrized as a function of Q_{30}) with the Coulomb repulsion barrier obtained in Sec. 3.2. The transition between the two regimes occur at the saddle point ($Q_{30} = 22 \text{ b}^{3/2}$ for ^{224}Ra , and $Q_{30} = 46 \text{ b}^{3/2}$ for ^{238}Pu), keeping the collective inertias consistent with the employed barrier.

The cluster-decay half-lives, computed from Eq. (5), are plotted in Fig. 5 for two different values of the collective zero-point energy E_0 . The comparison with experimental data [9] shows a good agreement when the GOA-GCM collective inertias are employed, while with the ATDHFB scheme the half-lives are overestimated (particularly for ^{238}Pu). In general, we notice a large scatter in the predicted results depending on the collective inertia scheme and E_0 value employed for the estimation of $t_{1/2}$. This is not a surprising result, as both nuclei have a high fission barrier (which in turn implies a small cluster emission probability and long half-life), which makes the theoretical calculations of $t_{1/2}$ extremely sensitive to the details concerning the estimation of the

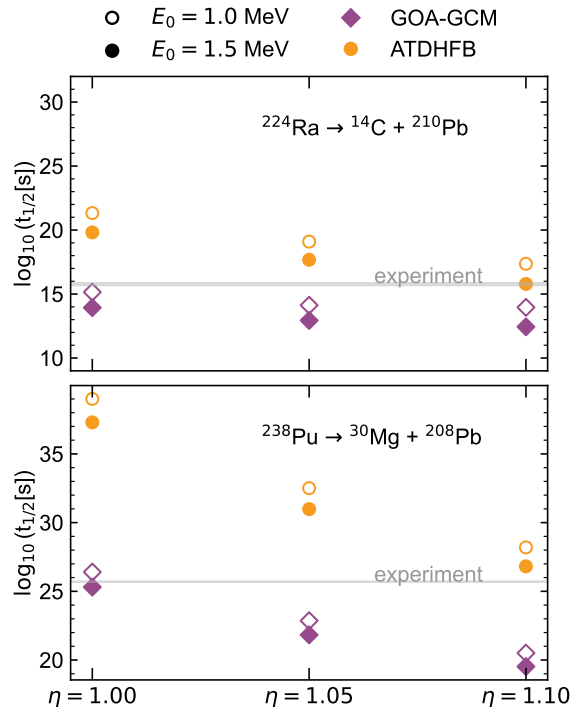


Fig. 5 Spontaneous fission half-lives for the cluster decay of ^{224}Ra (upper panel) and ^{238}Pu (lower panel) as a function of different values of the pairing strength η . Results obtained with ATDHFB collective inertias (6a) and GOA-GCM (6b) are plotted as orange circles and purple diamonds, respectively. Empty and full symbols represent the half-lives computed with $E_0 = 1.0$ and 1.5 , respectively. The horizontal gray band shows the experimental data [9].

quantities entering into Eq. (5). Regarding the absolute value of theoretical half-lives, it should be mentioned that the inclusion of pairing as collective degree of freedom can reduce the predicted $t_{1/2}$ of long-lived nuclei by several orders of magnitude [21, 34–36]. This is because collective inertias decrease as the square of the inverse pairing gap, leading to a reduction of the $t_{1/2}$ if the action integral in Eq. (5) is computed along the least-action path. While the inclusion of pairing as dynamical variable goes beyond the scope of this work, its effect on the collective inertias and $t_{1/2}$ can be mimicked by increasing the pairing strength η [20, 37, 38]. Fig. 5 shows the predicted half-lives for cluster emission when pairing strength is increased by 5% ($\eta = 1.05$) and 10% ($\eta = 1.10$). From this plot it is possible to conclude that for larger η values not only the $t_{1/2}$ are quenched, as expected, but also the spread in theoretical

predictions due to variations in E_0 and the collective inertia scheme is reduced, in agreement with the results obtained when pairing is included as collective degree of freedom [21, 35, 36]. Evidently, the choice of the collective inertia scheme is the main source of uncertainty, due to the large values of the collective action integral of these decays. While a better agreement with experimental data is obtained with the GOA-GCM scheme, as these are systematically smaller than the ATDHFB ones, an increase of the pairing strength by a 10% brings the ATDHFB predictions on top of experimental data, similarly to what already found in BCPM fission studies in transactinides nuclei [20]. However, we stress out again that theoretical $t_{1/2}$ are extremely sensitive to the details of the action integral calculation, and therefore the comparison with experimental data should be always taken with a grain of salt. Nevertheless, we conclude that BCPM provides a good reproduction of cluster decay half-lives within the simplified scheme presented in this work.

4 Conclusions

The cluster-decay properties of ^{224}Ra and ^{238}Pu have been computed using the BCPM EDF. By studying the evolution of the potential energy surface as a function of the mass quadrupole moment (elongation) and octupole moment (mass asymmetry) we identified the coexisting fission paths in these nuclei. Besides the traditional elongated fission mode, which proceeds through low values of the octupole moment, BCPM predicts the existence of a highly-asymmetric fission valley located at large Q_{30} , in agreement with previous EDFs studies [13]. The large value of the cluster barrier indicates that this mode is substantially suppressed compared to the traditional fission mode, as observed in laboratory.

The cluster decay half-lives are computed using the WKB formalism, by parametrizing the fission path as a function of Q_{30} . Due to the large values of the fission barriers, we find a large impact of collective inertias and ground-state zero-point energy on the estimated $t_{1/2}$. By increasing the pairing strength, the sensitivity of the estimated half-lives on the different quantities defining the collective action diminishes. Overall, a good agreement with experimental data is found when the GOA-GCM scheme is employed. Conversely, for

the ATDHFB inertias an increase in the pairing strength by a 10% is required in order to reproduce the observed $t_{1/2}$.

In a future work, we plan to expand and improve the formalism employed for the estimation of the half-lives. First and foremost, the impact of including pairing as a dynamical variable should be assessed, since it could reduce the predicted $t_{1/2}$ by several orders of magnitude. Furthermore, the estimation of the collective inertias can be improved by employing the non-perturbative ATDHFB and GOA-GCM schemes [39–41]. Work along these lines is in progress and will be the subject of a future publication.

Acknowledgments. Some figures shown in this paper were created following the color-blind friendly color scheme from Ref. [42]. This work has been supported by the Spanish Agencia Estatal de Investigación (AEI) of the Ministry of Science and Innovation (MCIN) under grant agreement No. PID2021-127890NB-I00. SG acknowledges support by the “Ramón y Cajal” grant No. RYC2021-031880-I funded by MCIN/AEI/10.13039/501100011033 and the European Union-“NextGenerationEU”.

References

- [1] A. Sandulescu, D.N. Poenaru, W. Greiner, New type of decay of heavy nuclei intermediate between fission and alpha decay. *Sov. J. Part. Nucl.* **11**(6) (1980). URL <https://www.osti.gov/biblio/6189038>
- [2] H.J. Rose, G.A. Jones, A new kind of natural radioactivity. *Nature* **307**(5948), 245–247 (1984). <https://doi.org/10.1038/307245a0>. URL <https://www.nature.com/articles/307245a0>
- [3] S.W. Barwick, P.B. Price, J.D. Stevenson, Radioactive decay of ^{232}U by ^{24}Ne emission. *Phys. Rev. C* **31**(5), 1984–1986 (1985). <https://doi.org/10.1103/PhysRevC.31.1984>. URL <https://link.aps.org/doi/10.1103/PhysRevC.31.1984>
- [4] P.B. Price, J.D. Stevenson, S.W. Barwick, H.L. Ravn, Discovery of Radioactive Decay of ^{222}Ra and ^{224}Ra by ^{14}C . *Phys. Rev. Lett.*

- 54(4), 297–299 (1985). <https://doi.org/10.1103/PhysRevLett.54.297>. URL <https://link.aps.org/doi/10.1103/PhysRevLett.54.297>
- [5] S. Wang, P.B. Price, S.W. Barwick, K.J. Moody, E.K. Hulet, Radioactive decay of ^{234}U via Ne and Mg emission. *Phys. Rev. C* **36**(6), 2717–2720 (1987). <https://doi.org/10.1103/PhysRevC.36.2717>. URL <https://link.aps.org/doi/10.1103/PhysRevC.36.2717>
- [6] S. Wang, D. Snowden-Ifft, P.B. Price, K.J. Moody, E.K. Hulet, Heavy fragment radioactivity of ^{238}Pu : Si and Mg emission. *Phys. Rev. C* **39**(4), 1647–1650 (1989). <https://doi.org/10.1103/PhysRevC.39.1647>. URL <https://link.aps.org/doi/10.1103/PhysRevC.39.1647>
- [7] P.B. Price, Heavy-Particle Radioactivity ($A > 4$). *Annu. Rev. Nucl. Part. Sci.* **39**(1), 19–42 (1989). <https://doi.org/10.1146/annurev.ns.39.120189.000315>. URL <https://www.annualreviews.org/doi/10.1146/annurev.ns.39.120189.000315>
- [8] R. Bonetti, C. Carbonini, A. Guglielmetti, M. Hussennois, D. Trubert, C. Le Naour, Cluster decay of ^{230}U via Ne emission. *Nucl. Phys. A* **686**(1-4), 64–70 (2001). [https://doi.org/10.1016/S0375-9474\(00\)00508-X](https://doi.org/10.1016/S0375-9474(00)00508-X). URL <https://linkinghub.elsevier.com/retrieve/pii/S037594740000508X>
- [9] R. Bonetti, A. Guglielmetti, Cluster radioactivity: an overview after twenty years. *Rom. Reports Phys.* **59**(2), 301 (2007)
- [10] A. Guglielmetti, D. Faccio, R. Bonetti, S.V. Shishkin, S.P. Tretyakova, S.V. Dmitriev, A.A. Ogloblin, G.A. Pik-Pichak, N.P. van der Meulen, G.F. Steyn, T.N. van der Walt, C. Vermeulen, D. McGee, Carbon radioactivity of ^{223}Ac and a search for nitrogen emission. *J. Phys. Conf. Ser.* **111**(1), 012050 (2008). <https://doi.org/10.1088/1742-6596/111/1/012050>. URL <https://iopscience.iop.org/article/10.1088/1742-6596/111/1/012050>
- [11] A. Bhagwat, Y.K. Gambhir, Relativistic mean field description of cluster radioactivity. *Phys. Rev. C* **71**(1), 017301 (2005). <https://doi.org/10.1103/PhysRevC.71.017301>. URL <https://link.aps.org/doi/10.1103/PhysRevC.71.017301>
- [12] F. Xu, J. Pei, Mean-field cluster potentials for various cluster decays. *Phys. Lett. B* **642**(4), 322–325 (2006). <https://doi.org/10.1016/j.physletb.2006.09.048>. URL <https://linkinghub.elsevier.com/retrieve/pii/S0370269306012275>
- [13] M. Warda, L.M. Robledo, Microscopic description of cluster radioactivity in actinide nuclei. *Phys. Rev. C* **84**(4), 44608 (2011). <https://doi.org/10.1103/PhysRevC.84.044608>. URL <http://link.aps.org/doi/10.1103/PhysRevC.84.044608>. arXiv:1107.1478
- [14] A. Adel, T. Alharbi, Cluster decay half-lives of trans-lead nuclei based on a finite-range nucleon–nucleon interaction. *Nucl. Phys. A* **958**, 187–201 (2017). <https://doi.org/10.1016/j.nuclphysa.2016.12.002>. URL <http://dx.doi.org/10.1016/j.nuclphysa.2016.12.002https://linkinghub.elsevier.com/retrieve/pii/S0375947416302986>
- [15] J. Zhao, J.P. Ebran, L. Heitz, E. Khan, F. Mercier, T. Nikšić, D. Vretenar, Microscopic description of α , 2α , and cluster decays of Rn 216–220 and Ra 220–224. *Phys. Rev. C* **107**(3), 1–9 (2023). <https://doi.org/10.1103/PhysRevC.107.034311>
- [16] M. Warda, A. Zdeb, L.M. Robledo, Cluster radioactivity in superheavy nuclei. *Phys. Rev. C* **98**(4), 041602 (2018). <https://doi.org/10.1103/PhysRevC.98.041602>. URL <http://arxiv.org/abs/1807.00342https://link.aps.org/doi/10.1103/PhysRevC.98.041602>. arXiv:1807.00342
- [17] Z. Matheson, S.A. Giuliani, W. Nazarewicz, J. Sadhukhan, N. Schunck, Cluster radioactivity of $^{294}_{118}\text{Og}_{176}$. *Phys. Rev. C* **99**(4), 041304 (2019). <https://doi.org/10.1103/PhysRevC.99.041304>. URL <https://link.aps.org/doi/10.1103/PhysRevC.99.041304>

- [18] S.A. Giuliani, Z. Matheson, W. Nazarewicz, E. Olsen, P.G. Reinhard, J. Sadhukhan, B. Schuetrumpf, N. Schunck, P. Schwerdtfeger, Colloquium : Superheavy elements: Oganesson and beyond. *Rev. Mod. Phys.* **91**(1), 011001 (2019). <https://doi.org/10.1103/RevModPhys.91.011001>. URL <https://doi.org/10.1103/RevModPhys.91.011001https://link.aps.org/doi/10.1103/RevModPhys.91.011001>
- [19] M. Baldo, L.M. Robledo, P. Schuck, X. Viñas, New Kohn-Sham density functional based on microscopic nuclear and neutron matter equations of state. *Phys. Rev. C* **87**(6), 064305 (2013). <https://doi.org/10.1103/PhysRevC.87.064305>. URL <http://arxiv.org/abs/1210.1321http://link.aps.org/doi/10.1103/PhysRevC.87.064305>. arXiv:1210.1321
- [20] S.A. Giuliani, L.M. Robledo, Fission properties of the Barcelona-Catania-Paris-Madrid energy density functional. *Phys. Rev. C* **88**(5), 054325 (2013). <https://doi.org/10.1103/PhysRevC.88.054325>. URL <https://link.aps.org/doi/10.1103/PhysRevC.88.054325>. arXiv:1305.0293 [nucl-th]
- [21] S.A. Giuliani, L.M. Robledo, R.R. Rodríguez-Guzmán, Dynamic versus static fission paths with realistic interactions. *Phys. Rev. C* **90**(5), 054311 (2014). <https://doi.org/10.1103/PhysRevC.90.054311>. URL <https://link.aps.org/doi/10.1103/PhysRevC.90.054311>. arXiv:1312.7229
- [22] S.A. Giuliani, G. Martínez-Pinedo, L.M. Robledo, Fission properties of superheavy nuclei for r-process calculations. *Phys. Rev. C* **97**(3), 034323 (2018). <https://doi.org/10.1103/PhysRevC.97.034323>. URL <https://link.aps.org/doi/10.1103/PhysRevC.97.034323>. arXiv:1704.00554
- [23] S.A. Giuliani, G. Martínez-Pinedo, M.R. Wu, L.M. Robledo, Fission and the r-process nucleosynthesis of translead nuclei in neutron star mergers. *Phys. Rev. C* **102**(4), 045804 (2020). <https://doi.org/10.1103/PhysRevC.102.045804>. URL <http://arxiv.org/abs/1904.03733https://link.aps.org/doi/10.1103/PhysRevC.102.045804>. arXiv:1904.03733
- [24] N. Schunck, L.M. Robledo, Microscopic theory of nuclear fission: A review. *Reports Prog. Phys.* **79**(11), 116301 (2016). <https://doi.org/10.1088/0034-4885/79/11/116301>. URL <http://arxiv.org/abs/1511.07517%0Ahttp://dx.doi.org/10.1088/0034-4885/79/11/116301http://stacks.iop.org/0034-4885/79/i=11/a=116301?key=crossref.30cd21ca9f619239da027337924f470b>. arXiv:1511.07517
- [25] N. Schunck, D. Regnier, Theory of nuclear fission. *Prog. Part. Nucl. Phys.* **125**, 103963 (2022). <https://doi.org/10.1016/j.pnpnp.2022.103963>. URL <https://doi.org/10.1016/j.pnpnp.2022.103963https://linkinghub.elsevier.com/retrieve/pii/S0146641022000242>. arXiv:2201.02719
- [26] L.M. Robledo, G.F. Bertsch, Application of the gradient method to Hartree-Fock-Bogoliubov theory. *Phys. Rev. C* **84**(1), 014312 (2011). <https://doi.org/10.1103/PhysRevC.84.014312>. URL <http://link.aps.org/doi/10.1103/PhysRevC.84.014312https://link.aps.org/doi/10.1103/PhysRevC.84.014312>. arXiv:1104.5453
- [27] M. Brack, J. Damgaard, A.S. Jensen, H.C. Pauli, V.M. Strutinsky, C.Y. Wong, Funny Hills: The Shell-Correction Approach to Nuclear Shell Effects and Its Applications to the Fission Process. *Rev. Mod. Phys.* **44**(2), 320–405 (1972). <https://doi.org/10.1103/RevModPhys.44.320>. URL <https://link.aps.org/doi/10.1103/RevModPhys.44.320>
- [28] M. Girod, B. Grammaticos, The zero-point energy correction and its effect on nuclear dynamics. *Nucl. Phys. A* **330**(1), 40–52 (1979). [https://doi.org/10.1016/0375-9474\(79\)90535-9](https://doi.org/10.1016/0375-9474(79)90535-9)
- [29] P. Ring, P. Schuck, *The Nuclear Many-Body Problem*, 1st edn. (Springer Berlin

- Heidelberg, Berlin, Heidelberg, 1980), pp. 1–718. URL <http://www.springer.com/us/book/9783540212065>
- [30] J.L. Egido, L.M. Robledo, in *Ext. Density Funct. Nucl. Struct. Phys.*, vol. 641, ed. by G. Lalazissis, P. Ring, D. Vretenar (Springer Berlin Heidelberg, Berlin, Heidelberg, 2004), chap. 10, pp. 269–302. https://doi.org/10.1007/978-3-540-39911-7_10. URL http://link.springer.com/10.1007/978-3-540-39911-7_10<http://arxiv.org/abs/nucl-th/0311106>
- [31] P. Reinhard, Zero-point energies in the two-center shell model. *Nucl. Phys. A* **252**(1), 133–140 (1975). [https://doi.org/10.1016/0375-9474\(75\)90607-7](https://doi.org/10.1016/0375-9474(75)90607-7). URL <https://linkinghub.elsevier.com/retrieve/pii/0375947475906077>
- [32] M. Baldo, L.M. Robledo, X. Viñas, The Barcelona Catania Paris Madrid energy density functional. *Eur. Phys. J. A* **59**(7), 156 (2023). <https://doi.org/10.1140/epja/s10050-023-01062-z>. URL <https://doi.org/10.1140/epja/s10050-023-01062-z><https://link.springer.com/10.1140/epja/s10050-023-01062-z>
- [33] M. Wang, W.J. Huang, F. Kondev, G. Audi, S. Naimi, The AME 2020 atomic mass evaluation (II). Tables, graphs and references. *Chinese Phys. C* **45**(3), 030003 (2021). <https://doi.org/10.1088/1674-1137/abddaf>. URL <https://iopscience.iop.org/article/10.1088/1674-1137/abddaf>
- [34] L.G. Moretto, R.P. Babinet, Large superfluidity enhancement in the penetration of the fission barrier. *Phys. Lett. B* **49**(2), 147–149 (1974). [https://doi.org/10.1016/0370-2693\(74\)90494-8](https://doi.org/10.1016/0370-2693(74)90494-8). URL <http://www.sciencedirect.com/science/article/pii/0370269374904948><http://linkinghub.elsevier.com/retrieve/pii/0370269374904948>
- [35] J. Sadhukhan, J. Dobaczewski, W. Nazarewicz, J.A. Sheikh, A. Baran, Pairing-induced speedup of nuclear spontaneous fission. *Phys. Rev. C* **90**, 1–5 (2014). <https://doi.org/10.1103/PhysRevC.90.061304>. URL <http://link.aps.org/doi/10.1103/PhysRevC.90.061304>
- [36] J. Zhao, B.N. Lu, T. Nikšić, D. Vretenar, S.G. Zhou, Multidimensionally-constrained relativistic mean-field study of spontaneous fission: Coupling between shape and pairing degrees of freedom. *Phys. Rev. C* **93**(4), 044315 (2016). <https://doi.org/10.1103/PhysRevC.93.044315>. URL <http://arxiv.org/abs/1603.00992><http://link.aps.org/doi/10.1103/PhysRevC.93.044315>. arXiv:1603.00992
- [37] R.R. Rodríguez-Guzmán, L.M. Robledo, Microscopic description of fission in uranium isotopes with the Gogny energy density functional. *Phys. Rev. C* **89**(5), 054310 (2014). <https://doi.org/10.1103/PhysRevC.89.054310>. URL <https://link.aps.org/doi/10.1103/PhysRevC.89.054310>. arXiv:1312.7229
- [38] R.R. Rodríguez-Guzmán, L.M. Robledo, Microscopic description of fission in neutron-rich plutonium isotopes with the Gogny-D1M energy density functional. *Eur. Phys. J. A* **50**(9), 142 (2014). <https://doi.org/10.1140/epja/i2014-14142-6>. URL <http://link.springer.com/10.1140/epja/i2014-14142-6>. arXiv:1405.6784
- [39] E. Yuldashbaeva, J. Libert, P. Quentin, M. Girod, Mass parameters for large amplitude collective motion: A perturbative microscopic approach. *Phys. Lett. B* **461**(1-2), 1–8 (1999). [https://doi.org/10.1016/S0370-2693\(99\)00836-9](https://doi.org/10.1016/S0370-2693(99)00836-9). URL <http://www.sciencedirect.com/science/article/pii/S0370269399008369><http://linkinghub.elsevier.com/retrieve/pii/S0370269399008369>
- [40] A. Baran, J.A. Sheikh, J. Dobaczewski, W. Nazarewicz, A. Staszczak, Quadrupole collective inertia in nuclear fission: Cranking approximation. *Phys. Rev. C* **84**(5), 054321 (2011). <https://doi.org/10.1103/PhysRevC.84.054321>. URL <https://link.aps.org/doi/10.1103/PhysRevC.84.054321>. arXiv:1007.3763

- [41] S.A. Giuliani, L.M. Robledo, Non-perturbative collective inertias for fission: A comparative study. *Phys. Lett. B* **787**, 134–140 (2018). <https://doi.org/10.1016/j.physletb.2018.10.045>.
URL <https://linkinghub.elsevier.com/retrieve/pii/S0370269318308165><http://www.sciencedirect.com/science/article/pii/S0370269318308165>
- [42] M.A. Petroff, Accessible Color Sequences for Data Visualization (2021). URL <http://arxiv.org/abs/2107.02270>. arXiv:2107.02270